

Article

Distribution of Glycerol Dialkyl Glycerol Tetraethers (GDGTs) in Carbonate-Type and Sulfate-Type Lacustrine Sediments: Insight into the Influence of Ionic Composition on GDGTs [†]

Yongxin Chen ¹, Xilong Zhang ¹, Wen Qi ², Gaoqing Zhang ³, Yu Pei ^{1,4}, Xuan Fang ¹, Yanqing Xia ^{1,*} and Shengyin Zhang ^{1,*} 

¹ Key Laboratory of Petroleum Resources, Northwest Institute of Eco-Environment and Resources, Chinese Academy of Sciences, Lanzhou 730000, China

² Research Institute of Petroleum Exploration and Development-Northwest (NWGI), PetroChina, Lanzhou 730020, China

³ College of Vanadium and Titanium, Panzhihua University, Panzhihua 617000, China

⁴ University of Chinese Academy of Sciences, Beijing 100049, China

* Correspondence: yqxia@lzb.ac.cn (Y.X.); zhangshengyin@nieer.ac.cn (S.Z.)

[†] Dedicated to our distinguished friend Prof. Baohua Chen on the occasion of his 60th birthday.

Abstract: The distribution of glycerol dialkyl glycerol tetraethers (GDGTs) in carbonate-type and sulfate-type saline lacustrine sediments from the Ordos Plateau in China is investigated to explore the influence of ionic composition on GDGTs. In general, they are relatively small (1.2–6.0 km² surface area) and shallow ponds (0.05–0.2 m water depth) and even seasonally dry lakes. The results reveal that the concentration of GDGTs has a good positive correlation with the (nCO₃²⁻ + nHCO₃⁻)/total ions, and the concentration of GDGTs in carbonate-type lake sediments is significantly higher than that in sulfate-type lake sediments. Most GDGT-based indices show no significant differences, and the distributions of GDGTs are similar in the two types of saline lake sediments. The lack of a positive correlation between the content of clay minerals and the concentration of GDGTs may imply that the ability of clay minerals to carry terrigenous organic matter is very limited in arid climates. The branched GDGTs (brGDGTs) in the two saline lake sediments may mainly come from in situ biological production and have low terrestrial inputs. The different weathering level of feldspar minerals in the two types of saline lakes results in the difference in organic matter content, which ultimately affects the concentration of GDGTs.

Keywords: carbonate-type saline lake; sulfate-type saline lake; ionic composition; GDGTs; reconstructed temperature



Citation: Chen, Y.; Zhang, X.; Qi, W.; Zhang, G.; Pei, Y.; Fang, X.; Xia, Y.; Zhang, S. Distribution of Glycerol Dialkyl Glycerol Tetraethers (GDGTs) in Carbonate-Type and Sulfate-Type Lacustrine Sediments: Insight into the Influence of Ionic Composition on GDGTs. *Minerals* **2022**, *12*, 1233. <https://doi.org/10.3390/min12101233>

Academic Editors: Qi Fu and Thomas Gentzis

Received: 14 August 2022

Accepted: 24 September 2022

Published: 28 September 2022

Publisher's Note: MDPI stays neutral with regard to jurisdictional claims in published maps and institutional affiliations.



Copyright: © 2022 by the authors. Licensee MDPI, Basel, Switzerland. This article is an open access article distributed under the terms and conditions of the Creative Commons Attribution (CC BY) license (<https://creativecommons.org/licenses/by/4.0/>).

1. Introduction

Biomarkers in sedimentary environments carry a lot of information about their producers and the environment, which may have the potential ability to record changes in global climate, environment, and vegetation at different temporal resolutions and are an important cornerstone for the reconstruction of paleoclimate and paleoecology [1,2]. A variety of biological and geochemical parameters, such as total organic carbon (TOC), tree rings, alkenone, pollen, $\delta^{18}\text{O}$, and *chironomus*, have been used to study climate and environmental change [3–5].

Over the last two decades, glycerol dialkyl glycerol tetraethers (GDGTs) (Figure S1) have attracted much attention and yielded a series of important research in climate reconstruction. They are membrane-spanning core lipids and are ubiquitous in soil, peat, rivers, oceans, sabkhas, and lakes [6–8]. Isoprenoid GDGTs (isoGDGTs) are derived from Archaea and have isoprenoid structures and 0–4 pentacyclic moieties. Among them, a special category of isoGDGTs is crenarchaeol (cren), which contains one cyclohexane and

four cyclopentanes, and is considered as a biomarker of Thaumarchaeota in water and soil [6]. In addition, the isomer of crenarchaeol (cren') usually accompanies it [9]. Branched GDGTs (brGDGTs) are derived from bacteria and have four to six methyl branches and 0–2 cyclopentane moieties [10–13]. GDGTs can respond sensitively to environmental changes (such as temperature, pH, or salinity) and adapt to various environments by changing the number of rings or methyl groups in the cell membrane structure, thus recording climate information in the form of different GDGTs [14,15]. A series of GDGT-based proxies have been established and widely used to record and reconstruct paleoclimate and paleoenvironmental changes in marine and terrestrial sediments [16–27].

Lacustrine facies are natural environments that are widely distributed in the world. Lake sediments have a wide geographical distribution range and good sedimentary continuity, which can provide multi-index records of different time scales and resolutions [28]. Therefore, they are a good vector for the reconstruction of regional paleoclimate and paleoenvironmental changes and play an important role in the study of paleoclimate and paleoenvironmental evolution in the Quaternary [29–31]. With the development of drilling technology in recent years, these lacustrine sediments provide continuous and high-resolution climate records from different locations, providing rich, global, comprehensive paleoenvironmental information [32,33].

However, due to the large spatial differences and complex physical and chemical environments of lacustrine systems (area, depth, basin morphology, salinity, pH, conductivity, etc.), there are still many difficulties in studying GDGTs in lakes. The conclusions obtained in different regions are irregular, and the reconstructed paleoclimatic and paleoenvironmental information of various proxies may be different, inconsistent, or even contradictory. For example, the tetraether index of 86 carbon atoms (TEX₈₆) failed to reconstruct lake surface temperature (LST) in many lacustrine systems, presumably because isoGDGTs in lake sediments were derived from other sources such as methanotrophs [18,34–36]. The MBT/CBT [13] indices are calculated based on the distribution of brGDGTs, using a combination of the methylation of branched tetraethers (MBT) and the cyclization of branched tetraethers (CBT). They are shown to correlate with mean annual air temperature (MAAT) in a global mineral soil dataset [15,17,37–39]. Due to the mixed sources of in situ production in lake waters, sediments, or allochthonous input from soils or rivers [11,17], seasonal variability in brGDGT production [40,41], and the regional differences among lakes, the application of soil-based MBT/CBT indices to lacustrine systems could systematically underestimate the MAAT. Hence, exhaustive studies of modern processes on the lake and the establishment of lake-specific temperature calibrations based on the study are required before applying the indicators, so as to clarify the information about the sedimentary environment and the distribution of GDGTs in the surface sediments to ensure the accuracy of reconstructed information [42–46].

As a product of special natural geographical conditions and geological environments, saline lake sediments are extremely sensitive to paleoclimate and paleoenvironment. In addition, saline lakes have often undergone an evolution from freshwater lakes to saltwater lakes. The various stages of saline lake evolution could record abundant information about climate and environmental evolution, even including information about salinization, which is lacking in ordinary freshwater lakes [47,48]. Therefore, it is meaningful to carry out paleoclimatic and paleoenvironmental reconstructions in saline lakes [46,49,50].

Saline lakes can be categorized into carbonate-type (also known as alkaline) or sulfate-type lakes based on the levels of eight major ions (Na^+ , K^+ , Mg^{2+} , Ca^{2+} , Cl^- , SO_4^{2-} , CO_3^{2-} , and HCO_3^-) [51,52]. In general, carbonate-type saline lakes, characterized by $K_{n1} = (\text{nCO}_3^{2-} + \text{nHCO}_3^-) / (\text{nCa}^{2+} + \text{nMg}^{2+}) > 1$ and $K_{n3} = \text{nSO}_4^{2-} / \text{nCa}^{2+} \gg 1$ [51,53], contain high levels of CO_3^{2-} or HCO_3^- and thus are depleted in Ca^{2+} , while sulfate-type saline lakes are enriched in Ca^{2+} and SO_4^{2-} and exhibit minimal levels of CO_3^{2-} . This disparity in ionic composition leads to significant differences in the composition, distribution, and evolution of clay minerals in the two types of saline lacustrine systems [53–56]. This divergence will eventually affect the formation and evolution of organic matter in those

saline lacustrine systems [57,58]. However, there is a lack of understanding about whether the ionic compositions of two types of saline lakes affect the generation and evolution of GDGTs. Therefore, this study selected two types of saline lakes from the Ordos Plateau in China to explore the influence of ionic composition on GDGTs and clarify the difference in GDGT concentrations, the distribution of GDGTs, and GDGT-based indices in both types of saline lacustrine systems. We also determined temperature calibrations suitable for the two types of saline lakes.

2. Materials and Methods

2.1. Study Areas

The Ordos Plateau is located in the south of the Inner Mongolia Autonomous Region and the east of the Ningxia Autonomous Region ($37^{\circ}20'–40^{\circ}0' N$; $106^{\circ}24'–111^{\circ}28' E$). It covers a total area of more than 120,000 km² and consists of the Loess Plateau in the south and the Ordos Desert in the north. The climate is warm and arid, with annual evaporation greatly exceeding precipitation [54]. There are more than fifty closed to semi-closed lakes in this region. These lakes have low seepage discharge with evaporation as the main water output.

Representative saline lakes were selected in the Ordos Plateau, NE China, with reference to Zheng [53,54]. The locations of the sampling sites are shown in Figure 1 and given in Table 1. Seven carbonate-type saline lake sediments (HH, DL, NL, HM, SU, HD, and DK) were taken as representative lakes in Otog Banner of Inner Mongolia, China (Figure 1c). An additional five sulfate-type saline lake sediments (GC, LN, BL, LH and HY) were taken as representative lakes from Dingbian in Shanxi Province, China, and a sixth, WH, was taken as a representative lake in Otag Qianqi of Inner Mongolia, China (Figure 1d). In general, they are relatively small (1.2–6.0 km² surface area) and shallow ponds (0.05–0.2 m water depth) and even seasonally dry lakes, located from 1300 to 1700 m above mean sea level. Most of lake basins were developed in the mid to late Holocene [53,54]. According to records of the meteorological stations in Otag Banner of Inner Mongolia from 1981 to 2010, the mean annual air temperature (MAAT), mean summer temperature (MSAT), mean winter temperature (MWAT), mean temperature of months above freezing (MAF) [59], and mean annual lake water temperature (MLWT) [60] of the carbonate-type lakes are approximately 7.5 °C, 21.5 °C, −7.6 °C, 12.6 °C, and 11.8 °C, respectively. The MAAT, MSAT, MWAT, MAF, and MLWT of carbonate lakes are about 8.8 °C, 21.6 °C, −5.3 °C, 13.5 °C, and 11.3 °C, respectively, according to records of the meteorological station in Otag Qianqi of Inner Mongolia and Dingbian of Shaanxi.

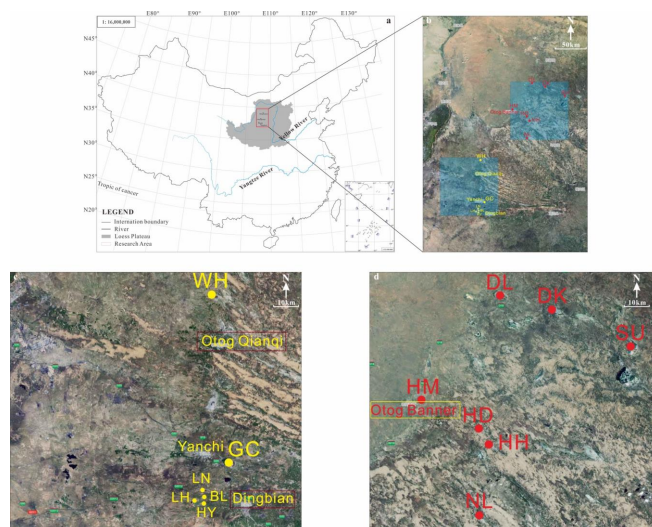


Figure 1. Location of the sampling sites in the Ordos Plateau, China. (a,b): Sketch map of the sampling basin/province. (c): Sampling location of sulfate-type saline lakes. (d): Sampling location of carbonate-type saline lakes. (Yellow dots, sulfate-type saline lakes; red dots, carbonate-type saline lakes).

Table 1. Geochemical data from surface sediments of the 13 saline lakes in the Ordos Basin.

Name	Location	Altitude (m)	Eight Main Ions Concentration (mg/L)								Type	Conductivity (ms/cm)	Salinity ^b (‰) ^b	TDS (ppm)	pH	TOC (%)	C/N Ratio
			K ⁺	Na ⁺	Ca ²⁺	Mg ²⁺	Cl ⁻	SO ₄ ²⁻	CO ₃ ²⁻	HCO ₃ ⁻							
HH	N: 38°56'13.38" E: 108°21'31.32"	1378	103.1	457.7	4.9	0.5	387.4	393.4	110.0	29.9	Carbonate-type lake	2.4	1.49	1140	9.1	0.03	0.8
DL	N: 39°28'36.06" E: 108°24'41.70"	1336	28.2	380.1	24.9	4.3	27.7	756.4	125.7	71.9	Carbonate-type lake	1.8	1.42	852	8.2	0.02	0.5
NL	N: 38°40'52.10" E: 108°18'49.32"	1344	2.9	547.4	0.0	84.4	269.5	237.0	120.0	4027.3	Carbonate-type lake	0.8	5.29	422	10.1	0.06	1.1
HM	N: 39°05'57.94" E: 108°02'32.46"	1353	274.2	36857.4	3.7	24.1	132,021.0	9729.5	22,107.4	18000.9	Carbonate-type lake	99.3	219.02	49,600	9.3	0.02	3.5
SU	N: 39°17'33.24" E: 109°01'16.20"	1334	101.6	392.9	185.3	1629.3	242.5	222.0	600.2	1322.1	Carbonate-type lake	1.2	4.70	580	9.8	0.06	2.8
HD	N: 38°59'46.44" E: 108°18'38.46"	1364	698.3	8219.4	22.8	-	5422.6	1191.6	5238.4	-	Carbonate-type lake	29.6	20.79	13,980	11.0	0.02	0.8
DK	N: 39°25'35.76" E: 108°39'12.78"	1342	106.3	3004.7	2.9	-	1521.7	970.0	1751.0	523.6	Carbonate-type lake	11.6	7.88	5140	10.4	0.19	5.7
WH	N: 38°21'41.70" E: 107°26'45.96"	1299	160.1	6830.9	1175.1	281.1	109,638.1	61,685.2	-	79.9	Sulfate-type lake	185.9	179.85	14,550	7.5	0.97	19.9
GC	N: 37°44'34.64" E: 107°31'21.55"	1301	43.3	21629.4	670.4	1155.8	59,227.0	26,200.0	-	610.2	Sulfate-type lake	53.2	109.54	26,600	8.5	0.11	7.8
LN	N: 37°38'27.30" E: 107°24'00.30"	1311	310.1	9429.6	867.3	3266.7	14,818.2	14,105.6	15.7	79.9	Sulfate-type lake	49.6	42.89	21,280	8.3	0.06	2.2
BL	N: 37°36'58.68" E: 107°24'29.46"	1326	199.1	11140.3	1160.1	2176.6	19,914.7	7290.5	39.3	47.9	Sulfate-type lake	57.4	41.97	26,750	8.2	0.32	14.7
LH	N: 37°36'10.92" E: 107°21'45.24"	1326	237.2	6394.5	1827.8	3703.7	18,235.7	8968.5	31.4	95.9	Sulfate-type lake	50	39.49	21,760	8.5	0.29	10.5
HY	N: 37°35'30.48" E: 107°24'24.00"	1332	115.6	7628.2	607.6	1929.0	8886.5	12,113.9	23.6	87.9	Sulfate-type lake	36.5	31.39	15,750	7.9	0.09	11.7

"-": indicates not detected. ^b: calculated as the sum of the measured ion.

In June 2017, 13 sediment samples (0–5 cm) near the lake center were obtained with a shovel. They were wrapped in aluminum foil and sealed bags. Each sample consisted of a homogenized mixture of three subsamples that were collected from each sampling point. After removing all plant residue and stones, the sediments were freeze dried and then ground to 200 mesh for further analysis.

2.2. Analysis of Hydrochemical Parameters

Because most saline lakes are dry saline lakes or small ponds, their water cannot be sampled. We thus measured the hydrochemical parameter compositions from sediments [56,61].

A sediment sample (50 g) was mixed with 250 mL of decarbonated water in a 500 mL polyethylene bottle, which was sealed and rigorously agitated at room temperature for 3 min. The supernatant was passed through a 0.45 μm filter, and the filtrate was stored in darkness at 4 $^{\circ}\text{C}$.

The concentrations of cations (Na^+ , K^+ , Mg^{2+} , and Ca^{2+}) were measured via inductively coupled plasma–optical emission spectrometry (ICP-OES; ThermoFisher ICAP6300, Waltham, MA, USA). The concentrations of anions (Cl^- , SO_4^{2-}) were measured using an ion chromatograph (Thermo-ICS 1500, USA) equipped with an AS11-HC analytical column (4 \times 250 mm; Dionex, Sunnyvale, CA, USA). The concentrations of HCO_3^- and CO_3^{2-} were determined via double indicator neutralization titration.

The conductivity and total dissolved solids (TDS) were determined via electrical conductivity (REX DDS-307, Shanghai INESA Scientific Instrument Co., Ltd, Shanghai, China). They were calibrated using standard solutions of KCl at 0.01 mol/L. Sediment pH was determined using a pH meter (Mettler Toledo FE20, Greifensee, Switzerland). The pH meter was calibrated against buffer standard solutions at pH values of 4.01, 7.00, and 9.00, with an error of $< \pm 0.03$ pH units. Salinity was calculated as the sum of the measured ions.

2.3. Analysis of Total Organic Carbon (TOC) and the C/N Ratio

The sample (3–5 g) was mixed with 3 M HCl to remove inorganic carbon and subsequently rinsed with deionized water until pH = 7. After freeze drying, the sample was analyzed to determine the TOC content and C/N ratio using an elemental analyzer (Elementar, Langensfeld, Germany).

2.4. X-ray Diffraction Analysis

Mineral compositions of sediment samples were determined using an Empyrean X-ray Diffractometer (Malvern Panalytical, Westborough, MA, USA) set to 30 kV and 40 mA. The mineralogy analyses were acquired from $2\theta = 5^{\circ}$ to $2\theta = 45^{\circ}$ at a scan rate of $2\theta = 2^{\circ}$ per min and an increment of $2\theta = 0.01^{\circ}$.

2.5. Analysis of Lipids

About 30 g of sample was extracted with dichloromethane (DCM)/methanol (MeOH) (9:1) using an accelerated solvent extractor (ASE100, Thermo, Waltham, MA, USA). The total lipid extracts (TLEs) were desulfurized with acid-activated copper powder and then concentrated. Subsequently, the TLEs were separated into apolar and polar fractions on a silica gel column by using hexane and DCM:MeOH (1:1), respectively. The polar fraction containing GDGTs was dissolved in DCM and filtered through a 0.45 μm (polytetrafluoroethylene) PTFE filter. The C46 standard was added for quantification [62].

GDGTs were analyzed using high-performance liquid chromatography with mass tandem spectrometry (HPLC MS/MS; Agilent 1200, Santa Clara, CA, USA) with auto-injection and ChemStation management software. The analysis conditions followed Yang [24]. 5- and 6-methyl brGDGTs were separated using two silica columns in tandem (150 mm \times 2.1 mm, 1.9 μm , Thermo Finnigan; San Jose, CA, USA) maintained at 40 $^{\circ}\text{C}$. Hexane and ethyl acetate were used as mobile phases A and B, respectively. The sample was redissolved in A/B = 84:16 (v/v). A 10 μL sample was injected and initially isocratic for the first 5 min with A/B = 84/16,

followed by an elution gradient from A/B = 84/16 to A/B = 82/18 from 5 min to 65 min and then to A/B = 0/100 from 65 min to 85 min, followed by A/B = 0/100 from 85 min to 90 min to wash the column and then back to A/B = 84/16 from 90 to 91 min, and finally equilibrated for 30 min. The flow rate was 0.2 mL/min. The GDGTs were ionized in an atmospheric pressure chemical ionization chamber with single-ion monitoring at mass/charge ratios (m/z) 1050, 1048, 1046, 1036, 1034, 1032, 1022, 1020, and 1018 for brGDGTs, and m/z 1302, 1300, 1298, 1296, and 1292 for isoGDGTs. The GDGTs were quantified from the integrated peak areas of the $[M+H]^+$ ions. The GDGT concentrations were then normalized to TOC.

2.6. GDGT-Based Indices

All calculation formulas for GDGTs are shown in Table S1.

2.7. Statistical Analysis

The correlation analysis and linear regressions were performed using SPSS 19.0 software. A p value < 0.05 indicated a significant correlation. Redundancy analysis (RDA) was performed using Canoco 5.0 software. The concentrations of GDGTs, fractional abundances of GDGTs, and GDGT-based indices were used as response variables; the hydrochemical parameters were used as explanatory variables; they were all transferred to the Canoco 5.0 software (Microcomputer Power, Ithaca, NY, USA).

3. Results and Discussion

3.1. Hydrochemical Parameters and TOC of Lake Sediments

All hydrochemical parameters are listed in Table 1 and Table S4. The pH values of the 13 lake sediments vary from 7.5 to 11.0, whereas sediments salinity varies from 1.42‰ to 219.02‰. The TOC varies from 0.02% to 0.97%. pH has linear correlations with $(nCO_3^{2-} + nHCO_3^-)/\text{total ions}$ ($r = 0.707$, $p < 0.001$) and $nSO_4^{2-}/\text{total ions}$ ($r = -0.768$, $p < 0.001$).

3.2. Concentrations and Distribution Patterns of isoGDGTs

The concentrations of individual isoGDGTs and total isoGDGTs and the fractional abundances of individual isoGDGTs are summarized in Table S2 and Figures 2 and 3.

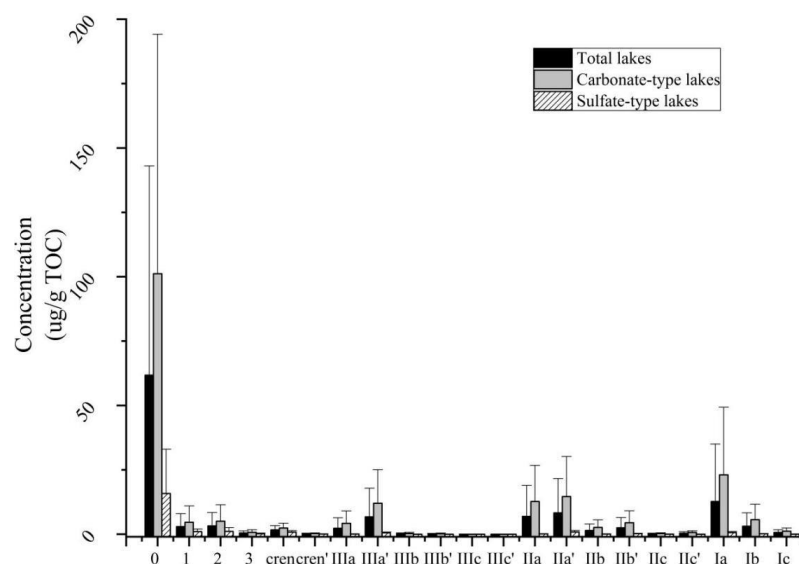


Figure 2. Concentrations of individual GDGTs in surface sediments.

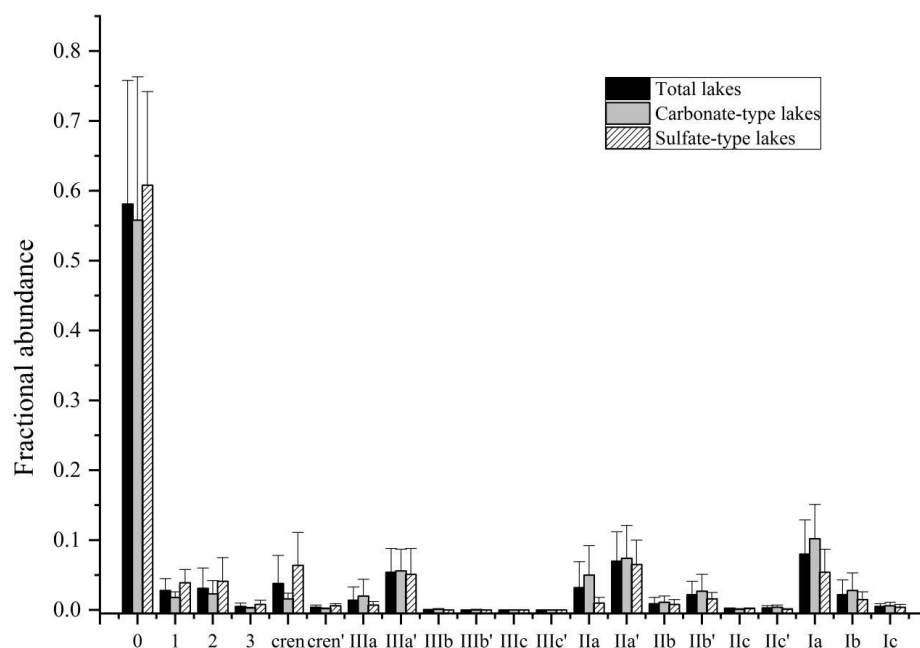


Figure 3. Fractional abundances of individual GDGTs in surface sediments.

Significant amounts of isoGDGTs are present in all samples. The concentration of isoGDGTs is highly variable, ranging from 3.02 $\mu\text{g/g}$ TOC to 336.61 $\mu\text{g/g}$ TOC, with an average of 69.11 $\mu\text{g/g}$ TOC. In carbonate-type lake sediments, the concentrations of isoGDGTs vary from 13.53 $\mu\text{g/g}$ TOC to 336.61 $\mu\text{g/g}$ TOC, with an average of 111.84 $\mu\text{g/g}$ TOC. In sulfate-type lake sediments, the concentrations of isoGDGTs vary from 3.02 $\mu\text{g/g}$ TOC to 54.61 $\mu\text{g/g}$ TOC, with an average of 19.26 $\mu\text{g/g}$ TOC. The concentration is generally higher in carbonate-type lake sediments compared to sulfate-type lake sediments (Figure 2).

The isoGDGT distributions of sediments are dominated by GDGT-0, consistent with previous studies of lacustrine sediments [7,35,50]. The average fractional abundance of GDGT-0 is 84.54% in sediments (Figure 3). The second most abundant isoGDGT is crenarchaeol, with an average proportion of 5.96%. The fractional abundance of isoGDGTs is generally slightly higher in carbonate-type lake sediments than in sulfate-type lake sediments.

3.3. Concentrations and Distribution Patterns of brGDGTs

The concentrations and distributions of typical brGDGTs in lake sediments are summarized in Table S3 and Figures 2 and 3.

The concentrations of total brGDGTs in lake sediments vary from 1.18 to 217.32 $\mu\text{g/g}$ TOC, with an average of 42.92 $\mu\text{g/g}$ TOC. Although the concentration of total brGDGTs is highly variable, it is almost always the case that the total concentration in carbonate-type samples is higher than that in sulfate-type samples. In carbonate-type samples, it ranges between 3.83 and 217.32 $\mu\text{g/g}$ TOC, with an average of 77.30 $\mu\text{g/g}$ TOC. In sulfate-type samples, it ranges from 1.18 $\mu\text{g/g}$ TOC to 5.24 $\mu\text{g/g}$ TOC, with an average of 2.88 $\mu\text{g/g}$ TOC.

The brGDGTs without cyclopentane moieties (IIIa and IIIa', IIa and IIa', and Ia) are generally more abundant than cyclopentane-ring-containing ones. Among them, pentamethylated brGDGTs (IIa and IIa') are generally the most abundant, followed by tetramethylated (Ia) and hexamethylated (IIIa and IIIa') brGDGTs. The fractional abundances of summed IIa and IIa' vary from 26.18% to 39.19%. This phenomenon also exists in the distributions of 5-Me or 6-Me brGDGTs. For example, IIa is almost always more abundant than IIIa. The exceptions are HM, DK, and LH, where the fractional abundances of summed Ia (34.82%–37.52%) are higher than those of summed IIa and IIa' (26.18%–30.81%). The abundance of 6-Me brGDGTs is generally higher than that of their isomer 5-Me brGDGTs. The isomer ratios of 6-Me brGDGT (IR_{6ME}) values (6-Me/5-Me brGDGTs) vary between

0.52 and 0.89. In summary, carbonate-type and sulfate-type lake sediments have similar brGDGT distributions.

3.4. GDGT Proxies

The GDGT-based proxies for all lake sediments are presented in Figure 4. The TEX_{86} values for carbonate-type lakes and sulfate-type lakes are almost identical at 0.57 ± 0.12 and 0.57 ± 0.11 , respectively. The archaeol and caldarchaeol ecometric (ACE) indices are also similar for the two types of lake sediments at 45.2 ± 15.1 and 43.2 ± 19.1 . The ratio of archaeal isoGDGTs to brGDGTs ($R_{i/b}$) for carbonate-type lakes is generally lower than that of sulfate-type lake sediments, with an average of 3.68 ± 4.23 in carbonate-type lakes and 6.57 ± 6.59 in sulfate-type lakes. The GDGT-0/cren values for the two types of lake sediments range from 10.60 to 108.45 in carbonate-type lakes and from 2.94 to 37.89 in sulfate-type lakes. The Cren/cren' values range from 6.34 to 10.08 in carbonate-type lakes and from 6.74 to 13.93 in sulfate-type lakes.

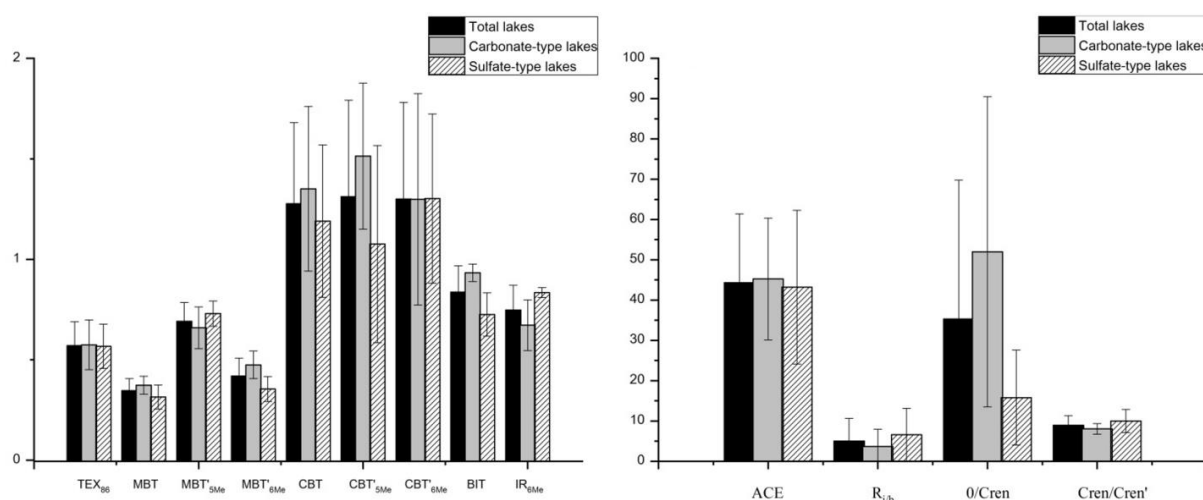


Figure 4. GDGT-based indices for the 13 surface sediments.

The MBT indices for carbonate-type lakes and sulfate-type lakes are similar at 0.37 ± 0.04 and 0.31 ± 0.06 , respectively. Due to the low concentrations of IIIb and IIIc in all samples, the MBT' indices are almost identical to those of MBT. The MBT'_{5Me} values for the two types of lakes are 0.66 ± 0.10 and 0.73 ± 0.06 , whereas the MBT'_{6Me} values are 0.47 ± 0.07 and 0.35 ± 0.06 . These differences between MBT'_{5Me} and MBT'_{6Me} may be due to the different biological communities producing 5- and 6-methyl brGDGTs and a predominance of the synthesis of 6-methyl brGDGTs in high-salinity environments [42]. The CBT indices for the two types of lakes are also similar. The original CBT indices in carbonate-type lakes and sulfate-type lakes are 1.35 ± 0.41 and 1.19 ± 0.38 , respectively; the CBT_{5Me} values in carbonate-type lakes and sulfate-type lakes are 1.51 ± 0.36 and 1.08 ± 0.49 , respectively; and the CBT_{6Me} values in carbonate-type lakes and sulfate-type lakes are 1.30 ± 0.53 and 1.30 ± 0.42 , respectively. The BIT index values in carbonate-type lakes are higher, at 0.93 ± 0.04 , than those in sulfate-type lakes, at 0.72 ± 0.11 . The IR_{6Me} values in carbonate-type lakes are lower, at 0.67 ± 0.13 , than those in sulfate-type lakes, at 0.83 ± 0.02 . Except for $R_{i/b}$, GDGT-0/cren, BIT, and IR_{6Me}, the indices show no significant differences between the two types of saline lakes.

3.5. The Influence of Saline Lake Type on GDGTs

3.5.1. Relationships between GDGTs and Hydrochemical Parameters in Surface Sediments

The significance test and RDA were performed to examine the impact of the proportions of the eight major ions ($(n\text{CO}_3^{2-} + n\text{HCO}_3^-)/\text{total ions}$, $n\text{SO}_4^{2-}/\text{total ions}$, and $(n\text{Ca}^{2+} + n\text{Mg}^{2+})/\text{total ions}$), salinity, and pH on the GDGT concentrations and distributions, and on GDGT-based indices (Figures 5 and 6). The results indicate that GDGT concentrations,

distributions, and GDGT-based indices are weakly correlated with sediment salinity. The best correlations are for GDGT concentrations and $(n\text{CO}_3^{2-} + n\text{HCO}_3^-)/\text{total ions}$.

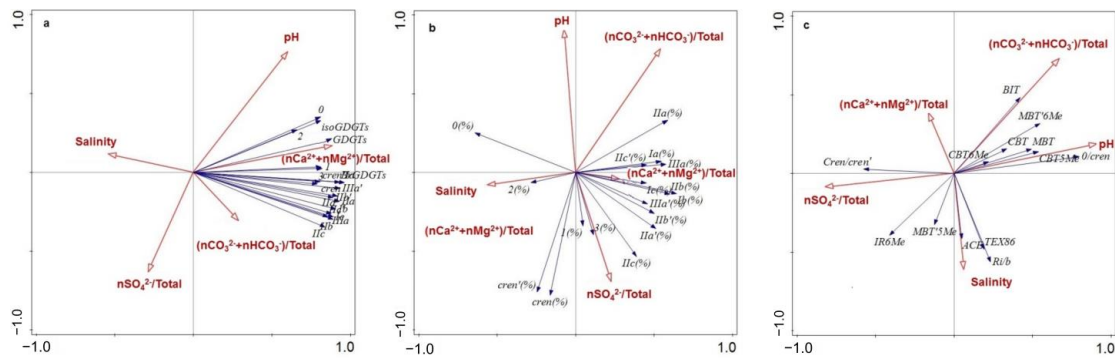


Figure 5. Redundancy analysis of the relationships between hydrochemical parameters with (a) GDGT concentrations, (b) GDGT distributions, and (c) GDGT-based indices.

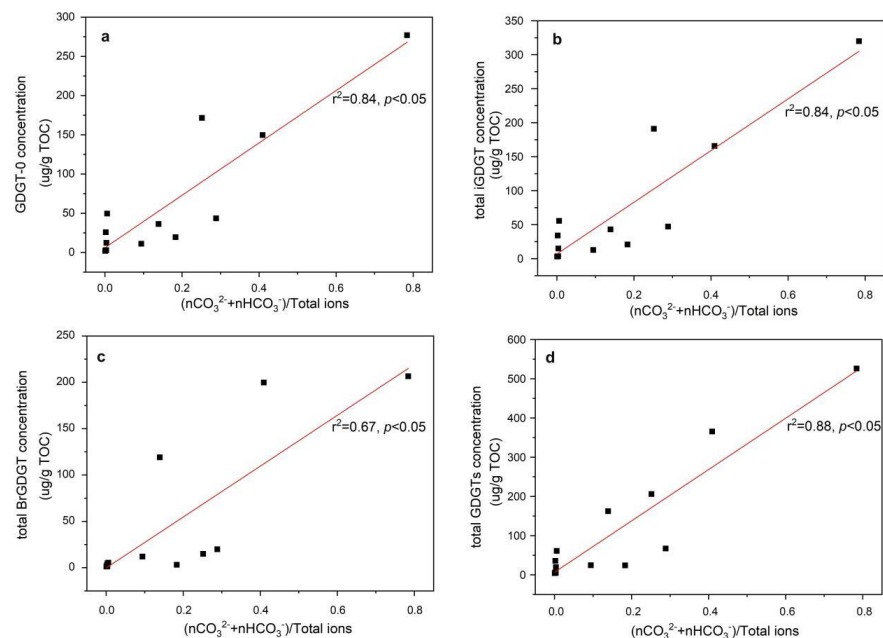


Figure 6. Plots of $(n\text{CO}_3^{2-} + n\text{HCO}_3^-)/\text{total ions}$ versus (a) GDGT-0 concentration, (b) total Igdgt concentration, (c) total BrGDGT concentration, (d) total GDGTs concentration.

The concentrations of GDGT-0, total isoGDGTs, and total GDGTs have good correlations with $(n\text{CO}_3^{2-} + n\text{HCO}_3^-)/\text{total ions}$ ($r = 0.90, p = 0.02$; $r = 0.91, p = 0.02$; and $r = 0.92, p = 0.02$, respectively). The concentrations of total brGDGTs, Iib', and cren have slightly weaker correlations with $(n\text{CO}_3^{2-} + n\text{HCO}_3^-)/\text{total ions}$ ($r = 0.82, p = 0.05$; $r = 0.75, p = 0.04$; and $r = 0.57, p = 0.004$, respectively). In contrast, $n\text{SO}_4^{2-}/\text{total ions}$, $(n\text{Ca}^{2+} + n\text{Mg}^{2+})/\text{total ions}$, pH, and salinity are insignificant factors in affecting GDGT concentrations. Among all the variables, the concentration of GDGT-0 showed the highest correlation with pH and $n\text{SO}_4^{2-}/\text{total ions}$ ($r = 0.70, p = 0.04$ and $r = -0.57, p = 0.02$). The Ic concentration has the best correlation with $(n\text{Ca}^{2+} + n\text{Mg}^{2+})/\text{total ions}$, although it is relatively weak ($r = 0.69, p = 0.006$). This may be because carbonate-type lakes contain more CO_3^{2-} and HCO_3^- than sulfate-type lakes, and the organic matter (mainly algae) contents are positively correlated with the concentrations of CO_3^{2-} and HCO_3^- [63]. As a result, the concentrations of GDGTs in carbonate-type lakes are higher than those in sulfate-type lakes, and there is a positive correlation between the concentrations of GDGTs and $(n\text{CO}_3^{2-} + n\text{HCO}_3^-)/\text{total ions}$.

The distributions of GDGTs are weakly correlated with all explanatory variables. Among them, the fractional abundance of cren' has weak negative correlations with pH ($r = -0.68, p < 0.001$) and $(nCO_3^{2-} + nHCO_3^-)/total\ ions$ ($r = -0.57, p = 0.03$). The fractional abundance of Iib' has the best correlation with $nSO_4^{2-}/total\ ions$ ($r = 0.63, p < 0.001$). The fractional abundance of each GDGTs is not well correlated with $(nCa^{2+} + nMg^{2+})/total\ ions$.

GDGT-based indices are also weakly correlated with all explanatory variables. Among them, 0/cren has weak correlations with pH ($r = 0.63, p = 0.02$), $(nCO_3^{2-} + nHCO_3^-)/total\ ions$ ($r = 0.62, p = 0.004$), and $nSO_4^{2-}/total\ ions$ ($r = -0.66, p = 0.004$). CBT'_{6ME} has a weak correlation with $(nCa^{2+} + nMg^{2+})/total\ ions$ ($r = 0.62, p = 0.006$).

3.5.2. Relationships between GDGTs and Mineralogy Characteristics in Surface Sediments

The linear relationship between feldspar content and GDGT concentrations observed in Figure 7a is not very good ($r^2 = 0.35$). However, it is also found that there is a certain positive correlation between feldspar content and GDGT concentrations by comparing Figures 7a and 8a,c. The content of feldspar in carbonate-type samples is higher than that in sulfate-type samples, and the corresponding concentration of GDGTs in carbonate-type samples is also higher than that in sulfate-type samples. This may be due to the low salt (Figure 7b) and high pH environment formed by the strong weathering of plagioclase and K-feldspar in carbonate salt lakes, which is conducive to plankton and soil microorganism growth [52,64,65]. However, feldspar minerals in sulfate-type saline lakes have weak weathering and a high concentration of sodium sulfate. Sodium stress and sulfate reduction inhibit microbial growth [66–68]. Thus, the concentration of GDGTs in the two types of salt lakes is different. The concentration of GDGTs in carbonate-type saline lake sediments is significantly higher than that in sulfate-type saline lake sediments.

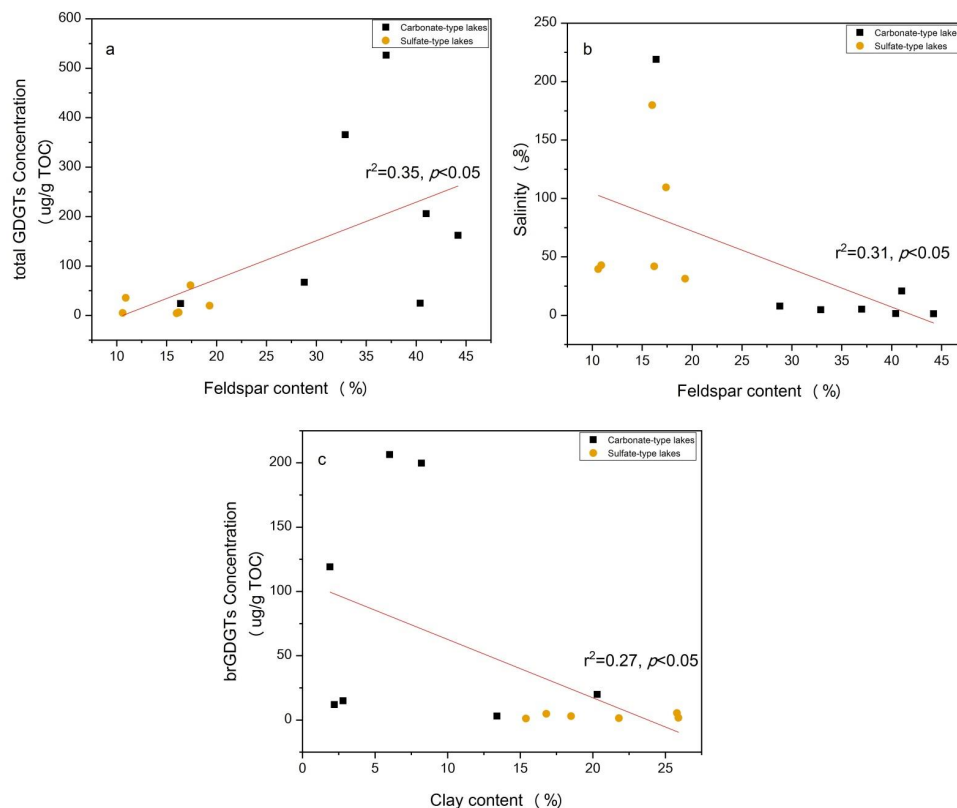


Figure 7. Comparison of (a) feldspar content and concentration of total GDGTs; (b) feldspar content and salinity; (c) clay content and concentration of brGDGTs in 13 surface sediments (feldspar content = Kfs + Pl).

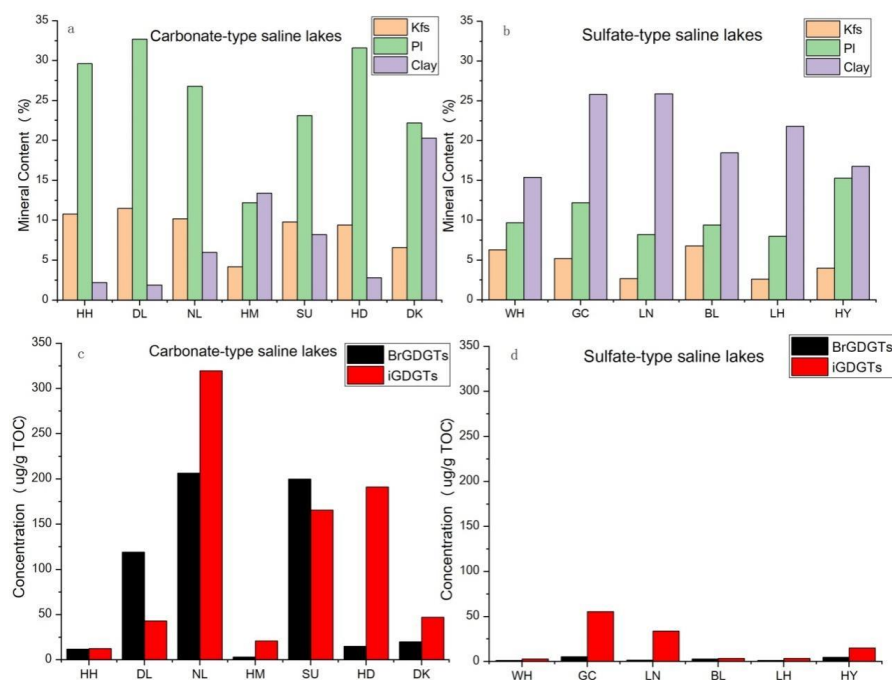


Figure 8. Comparison of mineral composition and concentration of GDGTs for 13 surface sediments. (a). mineral content of carbonate-type saline lake sediments; (b). mineral content of sulfate-type saline lake sediments; (c). GDGT concentrations in carbonate-type saline lake sediments; (d). GDGT concentrations in sulfate-type saline lake sediments.) (Kfs, K-feldspar; PI, plagioclase.)

On the other hand, compared with Figures 7c and 8b,d, the brGDGT concentration is weakly negatively correlated with clay mineral content. Generally speaking, the clay minerals in lake sediments mainly come from the surrounding soil, and the content of clay minerals should be positively correlated with the concentration of brGDGTs imported from terrigenous sources [69–71]. However, by comparing the relationship between the content of clay minerals and the concentration of brGDGTs, it can be found that although the content of sulfate-type clay minerals is high, there is no corresponding higher concentration of brGDGTs in sulfate-type samples than in carbonate-type samples. Therefore, it can be inferred that the ability of clay minerals to carry organic matter is very limited in arid climates, and the attachment relationship between organic matter and clay minerals is not as obvious as that of river-controlled lakes or offshore deposits. Therefore, it is possible that the organic matter in the sediments of the two types of lakes is mainly authigenic and low terrestrial inputs. There is no obvious difference between the parameters of the two types of saline lakes.

3.6. Performance of GDGT Proxies

3.6.1. BIT

The mean BIT index value for carbonate-type lakes is 0.93 ± 0.04 , and that for sulfate-type lakes is 0.72 ± 0.11 . Both types of saline lakes have quite high BIT values (>0.5), which is consistent with other lakes [8,16,34,72]. The study of Powers [16] and Blaga [34] showed that more than 75% of the global lakes have high BIT values (>0.5), especially those with small scales, which may be due to the fact that most brGDGTs are generated in situ in the water column or lake sediment [17,30,34,73,74]. Consequently, the BIT indices might not be suitable as indicators to trace the input of soil organic matter to aquatic environments.

3.6.2. Reconstruction of LST Based on TEX_{86}

We investigated the applicability of different TEX_{86} calibrations [16,30,75] to reconstruct the LST values of these saline lakes (Figure 9). The reconstructed temperatures in both types of saline lakes (approximately 15–19 °C) are significantly higher than the

recorded MAAT of 7.5 °C (carbonate-type saline lakes) and 8.8 °C (sulfate-type saline lakes), probably due to allochthonous and methanogen inputs [16,34,50,73]. The reconstructed summer lake surface temperatures [16] in carbonate-type and sulfate-type saline lakes are 21.18 °C ± 5.78 °C and 20.82 ± 5.12 °C, similar to the MSAT of 21.5 °C and 21.6 °C, respectively. Given that isoGDGTs are derived from allochthonous and methanogen inputs, we interpret that the agreement of the reconstructed summer lake surface temperature and MAST is a coincidence [16]. However, the TEX₈₆-reconstructed temperatures based on soil calibration [22] are −5.54 °C ± 5.58 °C and −5.88 °C ± 4.95 °C in carbonate-type and sulfate-type saline lakes, which are all lower than the observed MAAT. It can be seen that the TEX₈₆ indices are not suitable for LST reconstruction, probably due to the mixed source synthesized in the lake or derived from the surrounding alkaline soils.

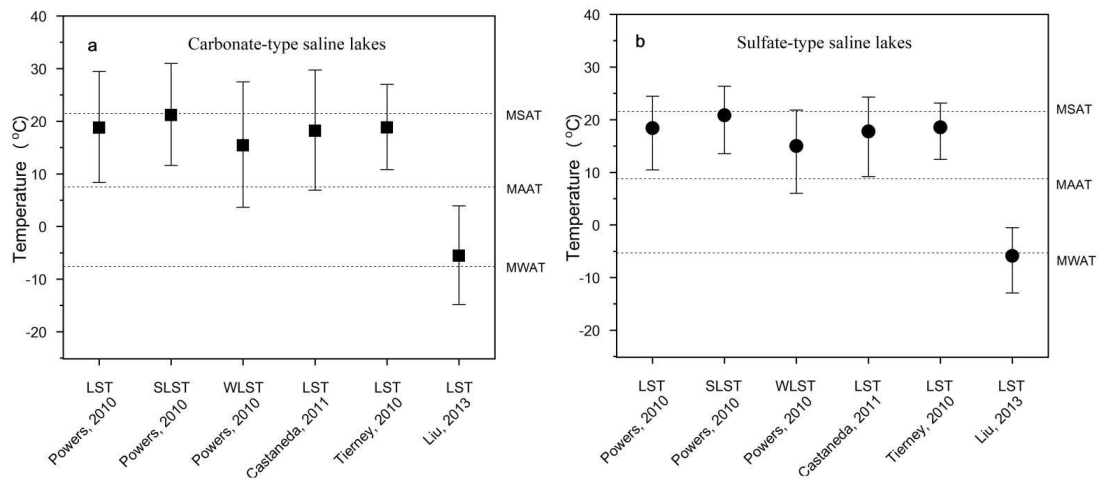


Figure 9. Comparison of reconstructed temperature based on different TEX86 calibrations as listed from formulas 14 to 19 in Table S1. (a): carbonate-type saline lakes and (b): sulfate-type saline lakes.

3.6.3. Reconstructed Temperature Based on the brGDGTs Indices

Through the above analysis, we infer that brGDGTs in both type of lakes are produced in situ, so various lake calibrations are applied to reconstruct temperature (Figure 10).

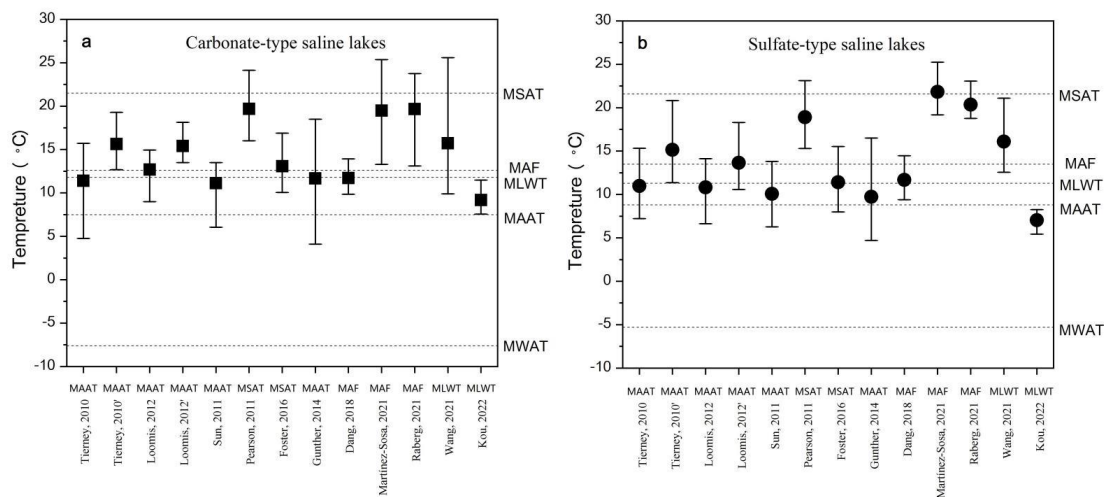


Figure 10. Comparison of reconstructed temperatures based on lake calibrations for different types of lakes as listed from formulas 20 to 32 in Table S1.

In carbonate-type saline lakes, the MBT/CBT calibration to African lakes yields temperatures at 11.39 °C ± 3.10 °C by Tierney [17] and 12.69 °C ± 1.75 °C by Loomis [19]. Applying the fractional abundances of the nine common brGDGTs reconstructs temper-

atures at $15.63\text{ }^{\circ}\text{C} \pm 1.97\text{ }^{\circ}\text{C}$ by Tierney [17] and $15.50\text{ }^{\circ}\text{C} \pm 1.37\text{ }^{\circ}\text{C}$ by Loomis [19]. When using the regional calibration to Chinese and Nepalese lakes [40], the reconstructed value obtained is $11.14\text{ }^{\circ}\text{C} \pm 2.25\text{ }^{\circ}\text{C}$. These reconstructed temperatures are all higher than the reported MAAT ($7.5\text{ }^{\circ}\text{C}$). Two calibrations established for lakes along a transect from the Scandinavian Arctic to Antarctica are applied. The reconstructed temperature is $19.69\text{ }^{\circ}\text{C} \pm 2.27\text{ }^{\circ}\text{C}$ using the calibration by Pearson [18], which is also higher than the recorded MAAT but similar to the MSAT ($21.5\text{ }^{\circ}\text{C}$). The calibration of Foster [25] yields a reconstructed temperature at $13.07\text{ }^{\circ}\text{C} \pm 2.03\text{ }^{\circ}\text{C}$, higher than the recorded MAAT but lower than the MSAT value. A calibration developed for the Tibetan Plateau [49] generates a reconstructed temperature with an average of $11.67\text{ }^{\circ}\text{C} \pm 4.21\text{ }^{\circ}\text{C}$, slightly higher than expected but with more variability. The newly developed calibration for 35 Chinese alkaline lake sediments [27] yields a reconstructed temperature at $11.72\text{ }^{\circ}\text{C} \pm 1.41\text{ }^{\circ}\text{C}$, which is slightly higher than the MAF ($12.6\text{ }^{\circ}\text{C}$) and only has slight variability. Employing the new calibrations to the MAF for global lakes reconstructs the temperature at $19.48\text{ }^{\circ}\text{C} \pm 3.45\text{ }^{\circ}\text{C}$ by Martínez-Sosa [44] and at $19.66\text{ }^{\circ}\text{C} \pm 3.16\text{ }^{\circ}\text{C}$ by Raberg [45], which are all higher than the recorded MAF. Furthermore, two calibrations to the MLWT for saline lakes from China are used. The reconstructed temperature is $15.72\text{ }^{\circ}\text{C} \pm 4.96\text{ }^{\circ}\text{C}$ by Wang [46], higher than the recorded MLWT ($11.8\text{ }^{\circ}\text{C}$), and $9.18\text{ }^{\circ}\text{C} \pm 1.23\text{ }^{\circ}\text{C}$ by Kou [42], slightly lower than the recorded MLWT.

The above temperature calibrations were also performed in sulfate-type saline lakes. Some temperature calibrations for African lakes were performed. The application of the MBT and CBT indices to reconstructed temperature yields a result of $10.97\text{ }^{\circ}\text{C} \pm 3.04\text{ }^{\circ}\text{C}$ by Tierney [17] and $10.82\text{ }^{\circ}\text{C} \pm 2.38\text{ }^{\circ}\text{C}$ by Loomis [19], which are slightly higher than the observed MAAT ($8.8\text{ }^{\circ}\text{C}$). Employing the fractional abundances of the nine common brGDGTs, the reconstructed temperature is $15.14\text{ }^{\circ}\text{C} \pm 3.03\text{ }^{\circ}\text{C}$ by Tierney and $13.66\text{ }^{\circ}\text{C} \pm 2.63\text{ }^{\circ}\text{C}$ by Loomis. The calibration for Chinese and Nepalese lakes [40] reconstructs a temperature of $10.08\text{ }^{\circ}\text{C} \pm 2.46\text{ }^{\circ}\text{C}$. Two calibrations for lakes along a transect from the Scandinavian Arctic to Antarctica are applied. The reconstructed temperature value is at $18.90\text{ }^{\circ}\text{C} \pm 2.84\text{ }^{\circ}\text{C}$ using the formula provided by Pearson [18], higher than the recorded MAAT but similar MSAT ($21.6\text{ }^{\circ}\text{C}$). Applying the calibration of Foster [25] yields a reconstructed temperature of $11.40\text{ }^{\circ}\text{C} \pm 2.59\text{ }^{\circ}\text{C}$, higher than the recorded MAAT but lower than the MSAT value. A calibration developed for Tibetan Plateau [49] yields the values of $9.73\text{ }^{\circ}\text{C} \pm 3.92\text{ }^{\circ}\text{C}$, slightly higher than expected but with more variability. The calibration for 35 Chinese alkaline lake sediments [27] reconstructs temperatures from $9.39\text{ }^{\circ}\text{C}$ to $14.47\text{ }^{\circ}\text{C}$, with an average of $11.67\text{ }^{\circ}\text{C} \pm 1.53\text{ }^{\circ}\text{C}$, which is slightly higher than expected and only has slight variability. Employing the calibrations to the MAF for global lakes generates the temperature of $21.82\text{ }^{\circ}\text{C} \pm 2.10\text{ }^{\circ}\text{C}$ by Martínez-Sosa [44] and $20.35\text{ }^{\circ}\text{C} \pm 1.66\text{ }^{\circ}\text{C}$ by Raberg [45], all higher than the recorded MAF. Furthermore, calibrations to the MLWT for saline lakes from China are used. The reconstructed values obtained are $16.10\text{ }^{\circ}\text{C} \pm 3.27\text{ }^{\circ}\text{C}$ by Wang [46], higher than the recorded MLWT ($11.8\text{ }^{\circ}\text{C}$), and $7.04\text{ }^{\circ}\text{C} \pm 1.11\text{ }^{\circ}\text{C}$ by Kou [42], slightly lower than the recorded MLWT.

In general, all the reconstructed temperatures are higher than the recorded MAAT. The calibration to MAF for 35 Chinese alkaline lake sediments is more accurate than other calibrations, which generates a temperature of $11.72\text{ }^{\circ}\text{C} \pm 1.41\text{ }^{\circ}\text{C}$ (MAF = $12.6\text{ }^{\circ}\text{C}$) in carbonate-type saline lakes and $11.67\text{ }^{\circ}\text{C} \pm 1.53\text{ }^{\circ}\text{C}$ (MAF = $13.5\text{ }^{\circ}\text{C}$) in sulfate-type saline lakes. In carbonate-type saline lakes, the calibrations to MLWT for Tibetan Plateau lakes also appears to be the more relevant, which yields a temperature of $9.18\text{ }^{\circ}\text{C} \pm 1.23\text{ }^{\circ}\text{C}$ (MLWT = $11.8\text{ }^{\circ}\text{C}$). In sulfate-type saline lakes, the calibration for Chinese and Nepalese lakes by Sun is more suitable, which reconstructs a temperature of $10.08\text{ }^{\circ}\text{C} \pm 2.46\text{ }^{\circ}\text{C}$ (MAAT = $8.8\text{ }^{\circ}\text{C}$).

4. Conclusions

We examined the distributions of GDGTs in different types of saline lakes from the Ordos Plateau in China. First, our work indicates that ionic composition has an effect on the

concentration of GDGTs. The concentrations of GDGTs in carbonate-type lake sediments are significantly higher than those in sulfate-type lake sediments, and their concentrations have good positive correlations with the $(n\text{CO}_3^{2-} + n\text{HCO}_3^-)/\text{total ions}$. Second, ionic composition has no obvious effect on the distribution of GDGTs and GDGT-based indices. The distribution of GDGTs is similar, and most GDGT-based indices show no significant differences between the two types of saline lakes. These characteristics may be caused by the different formation and evolution of the two types of saline lakes. Although the brGDGTs in two types of saline lakes may mainly come from in situ biological production, the different weathering levels of feldspar minerals lead to different organic matter content in the two types of saline lakes, and ultimately, to different concentrations of GDGTs.

Supplementary Materials: The following supporting information can be downloaded at: <https://www.mdpi.com/article/10.3390/min12101233/s1>, Figure S1: Structures and molecular ion mass/charge ratios (m/z) for glycerol dialkyl glycerol tetraethers (GDGTs); Table S1: Different calculation formulas for GDGTs; Table S2: Fractional abundances of individual isoGDGTs and the concentrations of total isoGDGTs for the 13 surface sediments; Table S3: Fractional abundances of individual brGDGTs and the concentrations of total brGDGTs and GDGTs for the 13 surface sediments; Table S4: The concentrations of major element for the 13 surface sediments.

Author Contributions: Conceptualization, Y.C.; W.Q.; and S.Z.; methodology, G.Z. and Y.P.; software, X.Z.; visualization, Y.C. and X.Z.; formal analysis, X.Z.; investigation, G.Z.; resources, X.Z.; W.Q.; G.Z., and X.F.; data curation, X.Z.; writing—original draft preparation, Y.C.; writing—review and editing, W.Q. and S.Z.; visualization, S.Z.; supervision, Y.X.; project administration, Y.X. and S.Z.; funding acquisition, Y.C. and X.Z. All authors have read and agreed to the published version of the manuscript.

Funding: This research was funded by the National Natural Science Foundation of China (42002174, 42102199); the Natural Science Foundation of Gansu Province (20JR10RA030, 21JR7RA062).

Data Availability Statement: Not applicable.

Acknowledgments: We are extremely grateful to Shijin Zhao and Hongye Pei for the GDGT analysis.

Conflicts of Interest: The authors declare no conflict of interest.

References

1. Gleixner, G.; Mügler, I. Compound-Specific Hydrogen Isotope Ratios of Biomarkers: Tracing Climatic Changes in the Past. In *Terrestrial Ecology*; Elsevier: Amsterdam, The Netherlands, 2007; pp. 249–265.
2. Naafs, B.D.A.; Inglis, G.N.; Blewett, J.; McClymont, E.L.; Lauretano, V.; Xie, S.; Evershed, R.P.; Pancost, R.D. The potential of biomarker proxies to trace climate, vegetation, and biogeochemical processes in peat: A review. *Glob. Planet. Change* **2019**, *179*, 57–79. [CrossRef]
3. Thompson, L.G.; Yao, T.; Mosley-Thompson, E.; Davis, M.E.; Henderson, K.A.; Lin, P.-N. A High-Resolution Millennial Record of the South Asian Monsoon from Himalayan Ice Cores. *Science* **2000**, *289*, 1916–1919. [CrossRef]
4. Esper, J.; Schweingruber, F.H.; Winiger, M. 1300 years of climatic history for Western Central Asia inferred from tree-rings. *Holocene* **2002**, *12*, 267–277. [CrossRef]
5. Wang, G.; Wang, Y.L.; Wei, Z.F.; He, W.; Zhang, T.; Ma, X.Y. Geochemical records of Qionghai Lake sediments in southwestern China linked to late Quaternary climate changes. *Palaeogeogr. Palaeoclimatol. Palaeoecol.* **2020**, *560*, 109902. [CrossRef]
6. Schouten, S.; Hopmans, E.C.; Sinninghe Damsté, J.S. The organic geochemistry of glycerol dialkyl glycerol tetraether lipids: A review. *Org. Geochem.* **2013**, *54*, 19–61. [CrossRef]
7. Wang, H.; Liu, W.; Zhang, C.; Wang, Z.; Wang, J.; Liu, Z.; Dong, H. Distribution of glycerol dialkyl glycerol tetraethers in surface sediments of Lake Qinghai and surrounding soil. *Org. Geochem.* **2012**, *47*, 78–87. [CrossRef]
8. Petrick, B.; Reuning, L.; Martínez-García, A. Distribution of Glycerol Dialkyl Glycerol Tetraethers (GDGTs) in Microbial Mats From Holocene and Miocene Sabkha Sediments. *Front. Earth Sci.* **2019**, *7*, 310. [CrossRef]
9. Leininger, S.; Urich, T.; Schloter, M.; Schwark, L.; Qi, J.; Nicol, G.W.; Prosser, J.I.; Schuster, S.C.; Schleper, C. Archaea predominate among ammonia-oxidizing prokaryotes in soils. *Nature* **2006**, *442*, 806–809. [CrossRef]
10. Sinninghe Damsté, J.S.; Hopmans, E.C.; Pancost, R.D.; Schouten, S.; Geenevasen, J.A.J. Newly discovered non-isoprenoid glycerol dialkyl glycerol tetraether lipids in sediments. *Chem. Commun.* **2000**, *17*, 1683–1684. [CrossRef]
11. Sinninghe Damsté, J.S.; Ossebaar, J.; Schouten, S.; Verschuren, D. Distribution of tetraether lipids in the 25-ka sedimentary record of Lake Challa: Extracting reliable TEX86 and MBT/CBT palaeotemperatures from an equatorial African lake. *Quat. Sci. Rev.* **2012**, *50*, 43–54. [CrossRef]

12. Sinninghe Damsté, J.S.; Rijpstra, W.I.C.; Hopmans, E.C.; Jung, M.-Y.; Kim, J.-G.; Rhee, S.-K.; Stieglmeier, M.; Schleper, C. Intact polar and core glycerol dibiphytanyl glycerol tetraether lipids of Group I.1a and I.1b Thaumarchaeota in soil. *Appl. Environ. Microb.* **2012**, *78*, 6866–6874. [[CrossRef](#)] [[PubMed](#)]
13. Weijers, J.W.H.; Schouten, S.; van den Donker, J.C.; Hopmans, E.C.; Sinninghe Damsté, J.S. Environmental controls on bacterial tetraether membrane lipid distribution in soils. *Geochim. Cosmochim. Acta* **2007**, *71*, 703–713. [[CrossRef](#)]
14. Schouten, S.; Hopmans, E.C.; Schefuß, E.; Sinninghe Damsté, J.S. Distributional variations in marine crenarchaeotal membrane lipids: A new tool for reconstructing ancient sea water temperatures? *Earth Planet. Sci. Lett.* **2002**, *204*, 265–274. [[CrossRef](#)]
15. De Jonge, C.; Hopmans, E.C.; Zell, C.I.; Kim, J.-H.; Schouten, S.; Sinninghe Damsté, J.S. Occurrence and abundance of 6-methyl branched glycerol dialkyl glycerol tetraethers in soils: Implications for palaeoclimate reconstruction. *Geochim. Cosmochim. Acta* **2014**, *141*, 97–112. [[CrossRef](#)]
16. Powers, L.A.; Werne, J.P.; Vanderwoude, A.J.; Sinninghe Damsté, J.S.; Hopmans, E.C.; Schouten, S. Applicability and calibration of the TEX86 paleothermometer in lakes. *Org. Geochem.* **2010**, *41*, 404–413. [[CrossRef](#)]
17. Tierney, J.E.; Russell, J.M.; Eggermont, H.; Hopmans, E.; Verschuren, D.; Sinninghe Damsté, J.S. Environmental controls on branched tetraether lipid distributions in tropical East African lake sediments. *Geochim. Cosmochim. Acta* **2010**, *74*, 4902–4918. [[CrossRef](#)]
18. Pearson, E.J.; Juggins, S.; Talbot, H.M.; Weckström, J.; Rosén, P.; Ryves, D.B.; Roberts, S.J.; Schmidt, R. A lacustrine GDGT-temperature calibration from the Scandinavian Arctic to Antarctic: Renewed potential for the application of GDGT-paleothermometry in lakes. *Geochim. Cosmochim. Acta* **2011**, *75*, 6225–6238. [[CrossRef](#)]
19. Loomis, S.E.; Russell, J.M.; Ladd, B.; Street-Perrott, F.A.; Sinninghe Damsté, J.S. Calibration and application of the branched GDGT temperature proxy on East African lake sediments. *Earth Planet. Sci. Lett.* **2012**, *357–358*, 277–288. [[CrossRef](#)]
20. Peterse, F.; van der Meer, J.; Schouten, S.; Weijers, J.W.; Fierer, N.; Jackson, R.B.; Kim, J.-H.; Sinninghe Damsté, J.S. Revised calibration of the MBT-CBT paleotemperature proxy based on branched tetraether membrane lipids in surface soils. *Geochim. Cosmochim. Acta* **2012**, *96*, 215–229. [[CrossRef](#)]
21. Xie, S.; Pancost, R.D.; Chen, L.; Evershed, R.P.; Yang, H.; Zhang, K.; Huang, J.; Xu, Y. Microbial lipid records of highly alkaline deposits and enhanced aridity associated with significant uplift of the Tibetan Plateau in the Late Miocene. *Geology* **2012**, *40*, 291–294. [[CrossRef](#)]
22. Liu, W.; Wang, H.; Zhang, C.L.; Liu, Z.; He, Y. Distribution of glycerol dialkyl glycerol tetraether lipids along an altitudinal transect on Mt. Xiangpi, NE Qinghai-Tibetan Plateau, China. *Org. Geochem.* **2013**, *57*, 76–83. [[CrossRef](#)]
23. Yang, H.; Pancost, R.D.; Dang, X.; Zhou, X.; Evershed, R.P.; Xiao, G.; Tang, C.; Gao, L.; Guo, Z.; Xie, S. Correlations between microbial tetraether lipids and environmental variables in Chinese soils: Optimizing the paleoreconstructions in semi-arid and arid regions. *Geochim. Cosmochim. Acta* **2014**, *126*, 49–69. [[CrossRef](#)]
24. Yang, H.; Lü, X.; Ding, W.; Lei, Y.; Dang, X.; Xie, S. The 6-methyl branched tetraethers significantly affect the performance of the methylation index (MBT') in soils from an altitudinal transect at Mount Shennongjia. *Org. Geochem.* **2015**, *82*, 42–53. [[CrossRef](#)]
25. Foster, L.C.; Pearson, E.J.; Juggins, S.; Hodgson, D.A.; Saunders, K.M.; Verleyen, E.; Roberts, S.J. Development of a regional glycerol dialkyl glycerol tetraether (GDGT)-temperature calibration for Antarctic and sub-Antarctic lakes. *Earth Planet. Sci. Lett.* **2016**, *433*, 370–379. [[CrossRef](#)]
26. Naafs, B.D.A.; Gallego-Sala, A.V.; Inglis, G.N.; Pancost, R.D. Refining the global branched glycerol dialkyl glycerol tetraether (brGDGT) soil temperature calibration. *Org. Geochem.* **2017**, *106*, 48–56. [[CrossRef](#)]
27. Dang, X.; Ding, W.; Yang, H.; Pancost, R.D.; David, B.; Naafs, A.; Xue, J.; Lin, X.; Lu, J.; Xie, S. Different temperature dependence of the bacterial brGDGT isomers in 35 Chinese lake sediments compared to that in soils. *Org. Geochem.* **2018**, *119*, 72–79. [[CrossRef](#)]
28. Bradley, R.S. *Paleoclimatology: Reconstructing Climates of the Quaternary*; Academic Press: Cambridge, MA, USA, 2014; Volume 4, pp. 11–13.
29. Last, W.M.; Smol, S.P. *Tracking Environmental Change Using Lake Sediments. Volume 2: Physical and Geochemical Method*; Springer: Berlin/Heidelberg, Germany, 2002.
30. Castañeda, I.S.; Schouten, S. A review of molecular organic proxies for examining modern and ancient lacustrine environments. *Quat. Sci. Rev.* **2011**, *30*, 2851–2891. [[CrossRef](#)]
31. Nurgul, B.; Yagmur, G.; Jérôme, K.; Sena, A.O.; Kadir, E.; Bradley, G.; Briony, H.N.H. Biotic and Abiotic Imprints on Mg-Rich Stromatolites: Lessons from Lake Salda, SW Turkey. *Geomicrobiol. J.* **2020**, *37*, 401–425.
32. Fawcett, P.J.; Werne, J.P.; Anderson, R.S.; Heikoop, J.M.; Brown, E.T.; Berke, M.A.; Smith, S.J.; Goff, F.; Donohoo-Hurley, L.; Cisneros-Dozal, L.M.; et al. Extended megadroughts in the southwestern United States during Pleistocene interglacials. *Nature* **2011**, *470*, 518–521. [[CrossRef](#)]
33. Wu, X.; Dong, H.; Zhang, C.; Liu, X.; Hou, W.; Zhang, J.; Jiang, H. Evaluation of glycerol dialkyl glycerol tetraether proxies for reconstruction of the paleo-environment on the Qinghai-Tibetan Plateau. *Org. Geochem.* **2013**, *61*, 45–56. [[CrossRef](#)]
34. Blaga, C.I.; Reichart, G.-J.; Heiri, O.; Sinninghe Damsté, J.S. Tetraether membrane lipid distributions in water-column particulate matter and sediments: A study of 47 European lakes along a north-south transect. *J. Paleolimnol.* **2009**, *41*, 523–540. [[CrossRef](#)]
35. Naeher, S.; Peterse, F.; Smittenberg, R.H.; Niemann, H.; Zigah, P.K.; Schubert, C.J. Sources of glycerol dialkyl glycerol tetraethers (GDGTs) in catchment soils, water column and sediments of Lake Rotsee (Switzerland) -implications for the application of GDGT-based proxies for lakes. *Org. Geochem.* **2014**, *66*, 164–173. [[CrossRef](#)]

36. He, Y.; Wang, H.; Meng, B.; Liu, H.; Zhou, A.; Song, M.; Kolpakova, M.; Krivonogov, S.; Liu, W.; Liu, Z. Appraisal of alkenone- and archaeal ether-based salinity indicators in mid-latitude Asian lakes. *Earth Planet. Sci. Lett.* **2020**, *538*, 116236. [[CrossRef](#)]
37. De Jonge, C.; Kuramae, E.E.; Radujković, D.; Weedon, J.T.; Janssens, I.A.; Peterse, F. The influence of soil chemistry on branched tetraether lipids in mid- and high latitude soils: Implications for brGDGT-based paleothermometry. *Geochim. Cosmochim. Acta* **2021**, *310*, 95–112. [[CrossRef](#)]
38. Halfman, R.; Lembrechts, J.; Radujković, D.; De Gruyter, J.; Nijs, I.; De Jonge, C. Soil chemistry, temperature and bacterial community composition drive brGDGT distributions along a subarctic elevation gradient. *Org. Geochem.* **2022**, *163*, 104346. [[CrossRef](#)]
39. Zang, J.; Lei, Y.; Yang, H. Distribution of glycerol ethers in Turpan soils: Implications for use of GDGT-based proxies in hot and dry regions. *Front. Earth Sci.* **2018**, *12*, 862–876. [[CrossRef](#)]
40. Sun, Q.; Chu, G.; Liu, M.; Xie, M.; Li, S.; Ling, Y.; Wang, X.; Shi, L.; Jia, G.; Lü, H. Distributions and temperature dependence of branched glycerol dialkyl glycerol tetraethers in recent lacustrine sediments from China and Nepal. *J. Geophys. Res.-Biogeosci.* **2011**, *116*, G01008.
41. Shanahan, T.M.; Hughen, K.A.; Van Mooy, B.A.S. Temperature sensitivity of branched and isoprenoid GDGTs in Arctic lakes. *Org. Geochem.* **2013**, *64*, 119–128. [[CrossRef](#)]
42. Kou, Q.; Zhu, L.; Ju, J.; Wang, J.; Xu, T.; Li, C.; Ma, Q. Influence of salinity on glycerol dialkyl glycerol tetraether-based indicators in Tibetan Plateau lakes: Implications for paleotemperature and paleosalinity reconstructions. *Palaeogeogr. Palaeoclimatol. Palaeoecol.* **2022**, *601*, 111127. [[CrossRef](#)]
43. Li, J.; Naafs, B.D.A.; Pancost, R.D.; Yang, H.; Liu, D.; Xie, S. Distribution of branched tetraether lipids in ponds from Inner Mongolia, NE China: Insight into the source of brGDGTs. *Org. Geochem.* **2017**, *112*, 127–136. [[CrossRef](#)]
44. Martínez-Sosa, P.; Tierney, J.E.; Stefanescu, I.C.; Dearing Crampton-Flood, E.; Shuman, B.N.; Routson, C. A global Bayesian temperature calibration for lacustrine brGDGTs. *Geochim. Cosmochim. Acta* **2021**, *305*, 87–105. [[CrossRef](#)]
45. Raberg, J.H.; Harning, D.J.; Crump, S.E.; De Wet, G.; Blumm, A.; Kopf, S.; Geirsdóttir, Á.; Miller, G.H.; Sepúlveda, J. Revised fractional abundances and warm-season temperatures substantially improve brGDGT calibrations in lake sediments. *Biogeosciences* **2021**, *18*, 3579–3603. [[CrossRef](#)]
46. Wang, H.; Liu, W.; He, Y.; Zhou, A.; Zhao, H.; Liu, H.; Cao, Y.; Hu, J.; Meng, B.; Jiang, J.; et al. Salinity-controlled isomerization of lacustrine brGDGTs impacts the associated MBT5ME' terrestrial temperature index. *Geochim. Cosmochim. Acta* **2021**, *305*, 33–48. [[CrossRef](#)]
47. Kezao, C.; Bowler, J.M. Late Pleistocene evolution of salt lakes in the Qaidam Basin, Qinghai province, China. *Palaeogeogr. Palaeoclimatol. Palaeoecol.* **1986**, *54*, 87–104. [[CrossRef](#)]
48. Rhodes, T.E.; Gasse, F.; Lin, R.; Fontes, J.-C.; Wei, K.; Bertrand, P.; Gibert, E.; Mélières, F.; Tucholka, P.; Wang, Z.; et al. A late Pleistocene-Holocene lacustrine record from lake Manas, Zunggar (Northern Xinjiang, Western China). *Palaeogeogr. Palaeoclimatol. Palaeoecol.* **1996**, *120*, 105–121. [[CrossRef](#)]
49. Günther, F.; Thiele, A.; Gleixner, G.; Xu, B.; Yao, T.; Schouten, S. Distribution of bacterial and archaeal ether lipids in soils and surface sediments of Tibetan lakes: Implications for GDGT-based proxies in saline high mountain lakes. *Org. Geochem.* **2014**, *67*, 19–30. [[CrossRef](#)]
50. Li, J.; Pancost, R.D.; Naafs, B.D.A.; Yang, H.; Zhao, C.; Xie, S. Distribution of glycerol dialkyl glycerol tetraether (GDGT) lipids in a hypersaline lake system. *Org. Geochem.* **2016**, *99*, 113–124. [[CrossRef](#)]
51. Valyashko, M.G. *Genesis of Brines in the Sedimentary Cove*; Akad. Nauk SSSR: Moscow, Russia, 1963; pp. 253–278.
52. Eugster, H.P. Lake Magadi, Kenya, and its precursors. In *Hypersaline Brines and Evaporitic Environments*; Nissenbaum, A., Ed.; Elsevier: Amsterdam, The Netherlands, 1980; pp. 195–232.
53. Zheng, X.Y. *Salt Saline Lakes of Inner Mongolia*; Science Press: Beijing, China, 1992.
54. Zheng, X.Y. *Saline Lakes of China Salt*; Science Press: Beijing, China, 2002.
55. Li, W.; Zhang, Y.Y.; Ni, M.J.; Tang, W.B. Genesis of alkaline lacustrine deposits in the Lower Permian Fencheng Formation of the Mahu Sag, northwestern Junggar Basin: Insight from a comparison with the worldwide alkaline lacustrine deposits. *Acta Geol. Sin.* **2020**, *94*, 1839–1852.
56. Qi, W.; Wu, J.; Xia, Y.; Zhang, X.; Li, Z.; Chang, J.; Bai, J. Influence of ionic composition on minerals and source rocks: An investigation between carbonate-type and sulfate-type lacustrine sediments based on hydrochemical classification. *Mar. Pet. Geol.* **2021**, *130*, 105099. [[CrossRef](#)]
57. Kennedy, M.J.; Löhr, S.C.; Fraser, S.A.; Baruch, E.T. Direct evidence for organic carbon preservation as clay-organic nanocomposites in a Devonian black shale; from deposition to diagenesis. *Earth Planet. Sci. Lett.* **2014**, *388*, 59–70. [[CrossRef](#)]
58. Rahman, H.M.; Kennedy, M.; Löhr, S.; Dewhurst, D.N.; Sherwood, N.; Yang, S.; Horsfield, B. The influence of shale depositional fabric on the kinetics of hydrocarbon generation through control of mineral surface contact area on clay catalysts. *Geochim. Cosmochim. Acta* **2018**, *220*, 429–448. [[CrossRef](#)]
59. Dearing Crampton-Flood, E.; Tierney, J.E.; Peterse, F.; Kirkels, F.M.; Damste, J.S.S. Baymbt: A bayesian calibration model for branched glycerol dialkyl glycerol tetraethers in soils and peats. *Geochim. Cosmochim. Acta.* **2020**, *68*, 142–159. [[CrossRef](#)]
60. Cao, J.; Rao, Z.; Shi, F.; Jia, G. Ice formation on lake surfaces in winter causes warm-season bias of lacustrine brGDGT temperature estimates. *Biogeosciences* **2020**, *17*, 2521–2536. [[CrossRef](#)]

61. Zhang, S.; Zhang, S.; Chen, Y.; Chen, B.; Lei, T. Distribution characteristics, source identification, and risk assessment of heavy metals in surface sediments of the salt lakes in the Ordos Plateau, China. *Environ. Sci. Pollut. Res.* **2022**, *216*, 1–13. [[CrossRef](#)] [[PubMed](#)]
62. Huguet, C.; Hopmans, E.C.; Febo-Ayala, W.; Thompson, D.H.; Sinninghe Damsté, J.S.; Schouten, S. An improved method to determine the absolute abundance of glycerol dibiphytanyl glycerol tetraether lipids. *Org. Geochem.* **2006**, *37*, 1036–1041. [[CrossRef](#)]
63. Bao, Y. *Study on Correlation between Phytoplankton Community Structure and its Environmental Factors in the Hamatai Lake and Chahannaer Lake in Etuoke*; Inner Mongolia Normal University: Hohhot, China, 2018; p. 27.
64. Cao, J.; Xia, L.; Wang, T.; Zhi, D.; Tang, Y.; Li, W. An alkaline lake in the Late Paleozoic Ice Age (LPIA): A review and new insights into paleoenvironment and hydrocarbon potential. *Earth-Sci. Rev.* **2020**, *202*, 103091. [[CrossRef](#)]
65. Kanzaki, Y.; Brantley, S.L.; Kump, L.R. A numerical examination of the effect of sulfide dissolution on silicate weathering. *Earth Planet. Sci. Lett.* **2020**, *539*, 116239. [[CrossRef](#)]
66. Sudhir, P.; Murthy, S.D.S. Effects of salt stress on basic processes of photosynthesis. *Photosynthetica* **2004**, *42*, 481–486. [[CrossRef](#)]
67. Rasool, S.; Hameed, A.; Azooz, M.M.; Muneeb-u-Rehman; Siddiqi, T.O.; Ahmad, P. Salt stress: Causes, types and responses of plants. In *Ecophysiology and Responses of Plants under Salt Stress*; Springer: New York, NY, USA, 2013; pp. 1–24.
68. Matsui, T.; Kojima, H.; Fukui, M. Effects of temperature on anaerobic decomposition of high-molecular weight organic matter under sulfate-reducing conditions. *Estuar. Coast. Shelf Sci.* **2013**, *119*, 139–144. [[CrossRef](#)]
69. Chukwuma, K.; Tsikos, H.; Wagner, N. Control of variability of primary grain assemblages on the stratigraphic differences in diagenetic processes and products in organic-rich sediments. *Sediment. Geol.* **2021**, *422*, 105966. [[CrossRef](#)]
70. Moal-Darrigade, P.; Ducassou, E.; Bout-Roumazielles, V.; Hanquiez, V.; Perello, M.-C.; Mulder, T.; Giraudeau, J. Source-to-sink pathways of clay minerals in the cadiz contourite system over the last 25 kyrs: The segregational role of mediterranean outflow water. *Mar. Geol.* **2022**, *443*, 106697. [[CrossRef](#)]
71. Novikau, R.; Lujaniene, G. Adsorption behaviour of pollutants: Heavy metals, radionuclides, organic pollutants, on clays and their minerals (raw, modified and treated): A review. *J. Environ. Manag.* **2022**, *309*, 114685. [[CrossRef](#)] [[PubMed](#)]
72. Tierney, J.E.; Russel, J.M. Distributions of branched GDGTs in a tropical lake system: Implications for lacustrine application of the MBT/CBT paleoproxy. *Org. Geochem.* **2009**, *40*, 1032–1036. [[CrossRef](#)]
73. Bechtel, A.; Smittenberg, R.H.; Bernasconi, S.M.; Schubert, C.J. Distribution of branched and isoprenoid tetraether lipids in an oligotrophic and a eutrophic Swiss lake: Insights into sources and GDGT-based proxies. *Org. Geochem.* **2010**, *41*, 822–832. [[CrossRef](#)]
74. Sinninghe Damsté, J.S.; Ossebaar, J.; Abbas, B.; Schouten, S.; Verschuren, D. Fluxes and distribution of tetraether lipids in an equatorial African lake: Constraints on the application of the TEX86 palaeothermometer and BIT index in lacustrine settings. *Geochim. Cosmochim. Acta* **2009**, *73*, 4232–4249. [[CrossRef](#)]
75. Tierney, J.E.; Mayes, M.T.; Meyer, N.; Johnson, C.; Swarzenski, P.W.; Cohen, A.S.; Russell, J.M. Late-twentieth-century warming in Lake Tanganyika unprecedented since AD 500. *Nat. Geosci.* **2010**, *3*, 422–425. [[CrossRef](#)]